Accepted for publication in 'Optical Materials'

Site occupancy determination of Eu/Y doped in Ca_2SnO_4 phosphor by electron channeling microanalysis

S. Muto* Y. Fujimichi and K. Tatsumi
Graduate School of Engineering, Nagoya University, Nagoya 464-8603, Japan

T. Kawano and H. Yamane
Institute of Multidisciplinary Research for Advanced Materials, Tohoku University, Sendai 980-8577, Japan

Abstract
Energy-dispersive X-ray analysis based on electron channeling effects in transmission electron microscopy (TEM) was performed on Ca_2SnO_4 phosphor materials doped with Eu^{3+}/Y^{3+} at various concentrations, which showed red photoluminescence associated with the Eu^{3+} $^5D_0$-$^7F_2$ electric dipole transition. The method provided direct information on which host element site impurity elements occupy. The local atomic configurations and chemical bonding states associated with dopant impurities with different ionic radii were also examined by TEM-electron energy-loss spectroscopy (TEM-EELS).

Keywords: rare-earth dopant, transmission electron microscopy, energy-dispersive X-ray analysis, electron energy-loss spectroscopy, electron channeling

1. Introduction

It is known that various types of oxide ceramic have been synthesized as phosphors by doping rare-earth activators into host ceramic materials. It is thus important to control the type and amount of atomic site that dopant rare-earth elements occupy and also to ensure that dopant impurities substitute for the host atom at the correct site as designed or to quantitatively measure the fraction of dopants that occupy crystallographic atomic sites.

It was reported [1,2] that Eu^{3+}-doped Ca_2SnO_4 exhibits strong photoluminescence (PL) derived from the $^5D_0$-$^7F_2$ electric dipole transition of Eu^{3+}. Yamane reported [3] that that Eu^{3+} equally occupies both the Ca^{2+} and Sn^{4+} sites, whose ionic radii are larger and smaller than Eu^{3+}, respectively by X-ray diffraction (XRD) and Rietveld analyses of the sample. The same authors' group also found that Ca_2SnO_4 codoped with Eu and Y of the same amount exhibits a stronger PL intensity than the sample single-doped with Eu, based on the idea that Y^{3+} ions with a smaller ionic radius preferentially occupy smaller cation (Sn^{4+}) sites, driving larger Eu^{3+} ions out of the Sn^{4+} site into the larger Ca^{2+} site [3,4]. The stronger PL in the codoped sample is explained by the increased fraction of Eu^{3+} ions occupying the Ca^{2+} site, because the Ca^{2+} site is coordinated by seven oxygen atoms, the asymmetric configuration of which enhances the electric dipole moment, compared with the symmetric six-coordinated Sn site. XRD-Rietveld analysis confirmed that preferential Ca^{2+} site occupation by Eu and Sn^{4+} site occupation by Y provided a small goodness-of-fit indicator of the Rietveld fit in the codoped samples [3,4], although it is not possible to determine the fraction of Eu(Y) that actually occupies the Ca^{2+}(Sn^{4+}) site.

In this study, samples with several dopant concentrations were synthesized and the site occupancies of rare-earth dopants were directly determined by energy-dispersive X-ray analysis

* Corresponding author: Tel: +81 52 789 5200 Fax: +81 52 789 4684 e-mail: s-mutoh@nucl.nagoya-u.ac.jp

(EDXA) combined with transmission electron microscopy (TEM), and the local spatial and electronic structure changes were also examined by electron energy loss spectroscopy (EELS).

2. Material and methods

2.1 Sample synthesis

Starting powders of $CaCO_3$ (99.99 %, Rare Metallic), SnO_2 (99.9 %, Sigma–Aldrich), Eu_2O_3 (99.99 %, Shin-Etsu Chem.) and Y_2O_3 (99.99 %, Nippon Yttrium) were weighed at molar ratios of Ca : Sn : Eu : Y = $2 - x$: $1 - x$: x : x (x = 0, 0.2, 0.5). Eu^{3+}-doped Ca_2SnO_4 with a composition of $Ca_{1.9}Eu_{0.2}Sn_{0.9}O_4$ was also prepared for reference. The powders were mixed in an agate mortar, pressed into pellets and placed on a platinum plate. The pellets were heated at 1400 °C for 24 h and then powdered for X-ray diffraction (XRD) analysis. This procedure (pelleting, heating and powdering) was repeated until no change in the XRD pattern was observed. The detailed sample synthesis procedures are reported in ref. 3. Samples of nominal compositions of Ca_2SnO_4 (nondoped), $Ca_{1.9}Eu_{0.2}Sn_{0.9}O_4$, $Ca_{1.8}Y_{0.2}Eu_{0.2}Sn_{0.8}O_4$, and $Ca_{1.5}Y_{0.5}Eu_{0.5}Sn_{0.5}O_4$, are hereafter referred to as nondoped, Eu20, Y20Eu20, and Y50Eu50, respectively.

$Ca_{1.8}Y_{0.2}Eu_{0.2}Sn_{0.8}O_4$ and $Ca_{1.9}Eu_{0.2}Sn_{0.9}O_4$ showed sharp red PL emissions at around 616 nm due to the $^5D_0$–$^7F_2$ electric dipole transition of Eu^{3+} ions excited with a 290 nm light [5]. The maximum intensity was observed for $Ca_{1.8}Y_{0.2}Eu_{0.2}Sn_{0.8}O_4$ (x = 0.2) and was around twofold higher than that of $Ca_{1.9}Eu_{0.2}Sn_{0.9}O_4$. More detailed X-ray analysis and PL results are reported elsewhere [5].

2.2 Transmission electron spectroscopy and associated analysis

The sintered pellet samples were cut into sheets of 2 x 2 x 0.5 mm^3, followed by dimpling at the center and Ar ion thinning to obtain thin areas transparent to high-energy incident electrons of TEM. TEM-EDX analysis was performed with a Hitachi H-800 TEM system (operated at 200 kV) equipped with an EDAX EDX system. The samples were also examined by EELS with a JEOL JEM2100 TEM system (operated at 200 kV) equipped with a Gatan Enfina 1000 spectrometer. Since the O-K energy-loss near edge structure (ELNES) showed significant variation for the Y50Eu50 sample (as shown in section 3.2), the extended energy-loss fine structure (EXELFS) of the O-K EELS was analyzed to examine the local atomic configuration around oxygen atoms [6].

2.3 Method for site occupancy determination

To determine the site occupancies of the rare-earth dopants, the statistical analysis method of electron channeling microanalytical data proposed by Rossouw *et al.* [7] was used: electron channeling for orientations under or near strong diffraction conditions results in standing waves that peak at different sites in the crystal unit cell and move as the crystal orientation with respect to the incident electron beam is varied. The crystal orientation dependence of Ca-K_α and Sn-L_α X-ray fluorescence yields around the [100] zone axis for Ca_2SnO_4 calculated by ICSC code [8] are shown in Figs. 1(a) and (b), respectively. It is seen that the X-ray intensity emitted from each site differently depends on the crystal orientation, and accordingly the characteristic X-ray intensities from impurities vary with the orientation, depending on which site they occupy. The X-ray count N_x for impurity x (in the present case, x = Eu or Y) can then be written in the following form [7,9] as a function of X-ray count N_i of host element i (e.g., i = Ca or Sn),

$$N_x = \frac{c_x}{k_k} \sum_i \frac{f_i k_i N_i}{(n_i - \sum_x c_x f_{ix})} = \sum_i \alpha_{ix} N_i \,, \qquad (1)$$

where

$$\alpha_{ix} = \frac{c_x}{k_k} \frac{f_i k_i}{(n_i - \sum_x c_x f_{ix})}, \qquad (2)$$

c_x is the concentration of impurity x, k_i is the k-factor of element i, n_i is the fraction of the cation site of element i among the total cation sites, and f_{ix} is the fraction of impurity x occupying the i-site. Many datasets of X-ray intensities from the cation elements (i.e., N_x, N_{Ca}, and N_{Sn}) are collected by tilting a sample by a few degrees at the same spot. α_{ix} can be derived from eq. (1) by a multivariate linear regression. α_{ix} can be derived from eq. (1) by a multivariate linear regression, because Eq.(1) stands for an equation of a flat plane in the (N_1, N_2,.., N_x) space. Then, c_x and f_{ix} can be derived utilizing $\sum_i f_{ix} = 1$ as

$$c_x = \sum_i \frac{\alpha_{ix} n_i}{(\sum_x \alpha_{ix} + k_i / k_x)}, \quad f_{ix} = \frac{\alpha_{ix} n_i}{c_x (\sum_x \alpha_{ix} + k_i / k_x)} \qquad (3)$$

Although the uncertainties in c_x and f_{ix} for multiple impurities have not been explicitly derived in ref. 9, they are readily estimated from the error propagation principle:

$$(\delta c_x)^2 = \sum_i \left[-\frac{\alpha_{ix} n_i}{(\sum_x \alpha_{ix} + k_i / k_x)^2} + \frac{n_i}{(\sum_x \alpha_{ix} + k_i / k_x)} \right]^2 (\delta \alpha_{ix})^2 \qquad (4)$$

$$(\delta f_{ix})^2 = \frac{1}{c_x^2} \left[-\frac{\alpha_{ix} n_i}{(\sum_x \alpha_{ix} + k_i / k_x)^2} + \frac{n_i}{(\sum_x \alpha_{ix} + k_i / k_x)} \right]^2 (\delta \alpha_{ix})^2 + \left(\frac{\delta c_x}{c_x^2} \right)^2 \left[\frac{\alpha_{ix} n_i}{(\sum_x \alpha_{ix} + k_i / k_x)} \right]^2 . \qquad (5)$$

We measured 20-30 datasets for one crystal grain by slightly tilting the sample consecutively around low–index zone axes within a few degrees; two different crystal grains were examined for each sample. Care was taken to obtain the EDX data at areas of similar thicknesses, that is, 100-150 nm, where electron channeling phenomena are strongly expected and X-ray emissions exhibit little significant difference in absorption effects within the thickness range. More detailed experimental conditions are described elsewhere [5].

It should be noted that since the Sn-L_β line (3.7 keV) overlaps with the Ca-K_α line, which significantly affects the intensity estimation of the Ca-K_α line, the intensity of the Ca-K_α line was calibrated by subtracting a fraction (0.55) of the neighboring Sn-L_α intensity [10].

3. Results and discussion

3.1 Site occupancies of rare-earth impurities

The coefficients α_{ix} (i = Ca, Sn, x = Eu, Y) derived using eq.(2), the site occupancies f_{ix} (eq.(3)) of the impurities and the impurity concentrations c of all the samples are tabulated in Table 1. The impurity concentrations are confirmed to be consistent with those nominal ones.

The resulting compositions are shown in Table 2, together with those obtained by XRD-Rietveld analysis [5]. In Eu20, Eu^{3+} equally occupies the Ca^{2+} and Sn^{4+} sites ensuring the charge neutrality condition, which is consistent with the results of XRD-Rietveld analysis. On the other hand, in the codoped samples, Eu^{3+} and Y^{3+} occupied the Ca^{2+} and Sn^{4+} sites at fractions of approximately 7:3 and 4:6, respectively, without resulting in a complete bias for a single site by a single element, which maintained the charge neutrality condition within the present experimental accuracies, as shown in the bottom row of Table 2.

3.2 Electron energy-loss spectroscopy

To seek a specific reason for the start of PL intensity decrease at dopant concentrations larger than 7at% [5] other than the general concentration quenching. We examined the local chemical states around the constituent elements. The ELNES of Ca-$L_{2,3}$, Y-$L_{2,3}$ and Eu-$M_{4,5}$ exhibited no dependence on dopant concentration. In addition, the results of high-angular resolution channeling enhanced EELS (HARECES) [11] of Y-$L_{2,3}$ and Eu-$M_{4,5}$ ELNES indicated that the rare-earth dopants were trivalent, independent of the type of atomic site occupied. On the other hand, Fig. 2 shows that O-K ELNES of the Y50Eu50 sample exhibited a blunt nature compared with that of the other samples, which can be caused by either local lattice distortions around oxygen or an increased concentration of dopant-oxygen pairs.

To confirm whether local lattice distortions around oxygen atoms are present, the extended energy-loss fine structures (EXELFSs) of the O-K edges of the nondoped and Y50Eu50 samples were compared. The EXELFS interference function, $\chi(k)$ was extracted in the same manner as in EXAFS analysis by subtracting the post-edge background from the oxygen K-shell EEL spectra recorded up to 900 eV and then normalizing the remaining signal by the post-edge background. The origin of the wave number k was set at the inflection point of the edge onset [6]. The $k\chi(k)$'s of both samples are shown in Fig. 3, indicating no appreciable changes in the local bond lengths except for a slight decrease in the wavelength of the main oscillating component, reflecting an increase in the lattice constants associated with the doping of oversized ions. It is thus considered that the blunt O-K ELNES of the Eu50Y50 sample is ascribed to the overlapping of multiple chemical states revealed by the increased dopant concentrations, rather than to local lattice distortions associated with the heavy doping.

4. Conclusions

The present electron channeling microanalysis directly confirmed that Eu^{3+} occupies both the Ca^{2+} and Sn^{4+} sites in the Eu20 sample; however, in the codoped samples, the site occupancies are slightly biased so that the dopant atoms preferentially occupy cation sites with an ionic radius larger than theirs. This clearly explains the enhancement of PL intensity associated with the electric dipole transition in Eu^{3+} by codoping with Y^{3+} up to a certain concentration, although we presently found no specific reason for the start of PL intensity decrease at dopant concentrations larger than $x = 0.20$ (20at%) in $Ca_{2-x}Y_xEu_xSn_{1-x}O_4$ other than the general concentration quenching.

Acknowledgment

This work was supported in part by the Global COE Program "Materials Integration, Tohoku University" and a Grant-in-Aid for Scientific Research (KAKENHI) in Priority Areas (#474) "Atomic Scale Modification."

References

[1] Y.-C. Chen, Y.-H. Chang, B.-S. Tsai, Opt. Mater. 27 (2005) 1874–1878.
[2] H. M. Yang, J. X. Shi, M. L. Gong, J. Sol. State. Chem. 178 (2005) 917–920.
[3] H. Yamane, Y. Kaminaga, S. Abe and T. Yamada, J. Solid State Chem. 181 (2008) 2559-2564.
[4] H. Yamane, T. Yamada and T. Kawano, Mater. Integ. 22 (2009) 6-11 (in Japanese).
[5] Y. Fujimichi, S. Muto, K. Tatsumi, T. Kawano and H. Yamane, J. Sol. Stat. Chem. 183 (2010) 2127-2132.
[6] Y. Kobayashi, S. Muto, C. Echer and T. Tanabe, J. Electron Microsc. 48 (1999) 525-529.
[7] C. J. Rossouw, P. S. Turner, T. J. White and A. J. O'Cornner, Phil. Mag. Lett. 60 (1989) 225-132.
[8] M. P. Oxley and L. J. Allen, J. Appl. Cryst. 36 (2003) 940-943.

[9] P. S. Turner, T. J. White, A. J. O'Conner and C. J. Rossouw, J. Microsc. 162 (1991) 369-378.
[10] A. Thompson, et al., (ed.), *X-ray Data Booklet*, Center for X-ray Optics and Advanced Light Source, Lawrence Berkeley National Laboratory, 2001, Table 1-3.
[11] K. Tatsumi, S. Muto, I. Nishida and J. Rusz, Appl. Phys. Lett. 96 (2010) 201911 (3 pages).

Table 1. Derived parameters (defined in text) of the samples of Eu20, Eu20Y20 and Eu50Y50.

Sample	Dopant	α_{Ca}	α_{Sn}	f_{Ca}	f_{Sn}	C_i (i = Eu or Y)
Eu20	Eu	0.070(8)	0.119(14)	0.51(7)	0.49(6)	0.0065(5)
Eu20Y20	Eu	0.112(10)	0.093(15)	0.70(6)	0.30(8)	0.071(6)
	Y	0.050(12)	0.147(19)	0.40(11)	0.60(11)	0.079(10)
Eu50Y50	Eu	0.303(13)	0.298(31)	0.69(5)	0.31(5)	0.159(7)
	Y	0.107(15)	0.369(34)	0.39(6)	0.61(5)	0.149(12)

TABLE 2. Compositions of the evaluated samples of Eu20, Eu20Y20 and Eu50Y50. The values in square brackets are XRD-Rietveld results [3].

Site	Element	nondoped Ca_2SnO_4	Eu20	Eu20Y20	Eu50Y50
Ca	Ca	2.00	1.89(1) [1.90]	1.77(4) [1.80]	1.46(4) [1.50]
	Eu	-	0.11(1) [0.10]	0.15(2) [0.20]	0.36(2) [0.50]
	Y	-	-	0.08(2) [0.0]	0.18(2) [0.0]
Sn	Sn	1.00	0.91(1) [0.90]	0.83(4) [0.80]	0.54(4) [0.50]
	Eu	-	0.09(1) [0.10]	0.05(2) [0.0]	0.14(2) [0.0]
	Y	-	-	0.12(2) [0.20]	0.32(2) [0.50]
Total charge per chemical formula		0	+0.010(25)	+0.038(77)	+0.086(108)

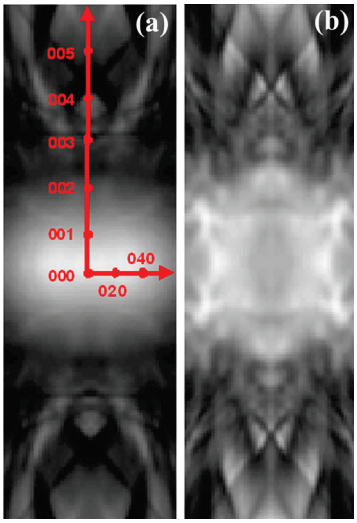

Fig. 1 The crystal orientation dependence of Ca-K_α (a) and Sn-L_α (b) X-ray fluorescence yields around the [100] zone axis for Ca_2SnO_4 calculated by ICSC code [6]. The coordinates inset in (a) are the Bragg spots corresponding for the tilting angles about the [100] zone axis.

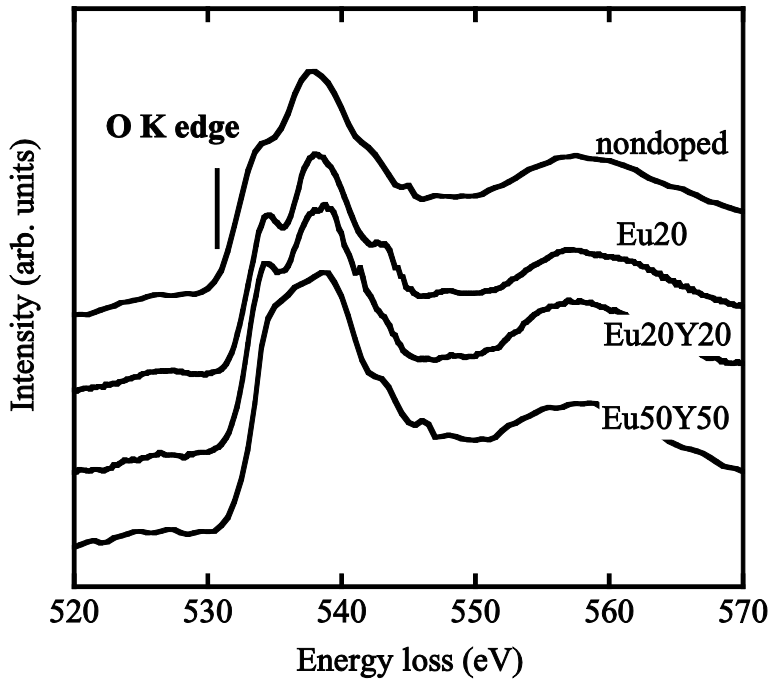

Fig. 2 Electron energy-loss spectra of O K for the present samples as indicated.

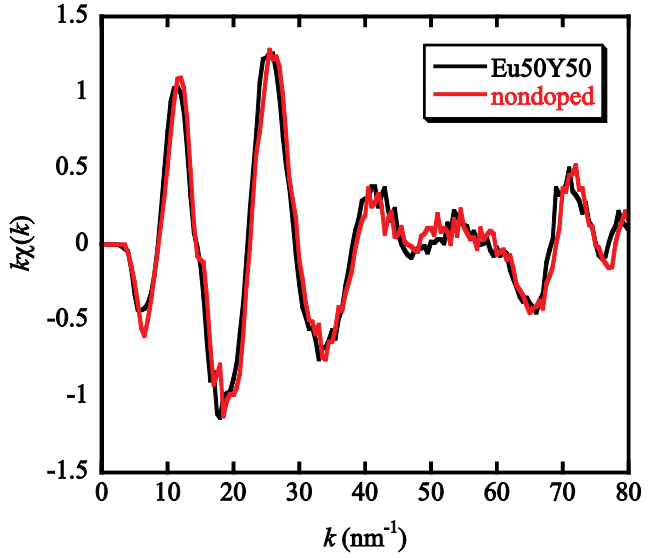

Fig. 3 EXELFS interference functions $\chi(k)$ extracted from the O K EEL spectra of nondoped and Eu50Y50 samples. k stands for the wave number in unit of nm^{-1}.